SAND80-0679
Unlimited Release
UC-70

Thermal Conductivity of Silicic Tuffs: Predictive Formalism and Comparison With Preliminary Experimental Results

Allen R. Lappin

Prepared by Sandia Laboratories, Albuquerque, New Mexico 87185
and Livermore, California 94550 for the United States Department
of Energy under Contract DE-AC04-76DP00789

Printed July 1980

Sandia National Laboratories

F 2900-Q(3-80)

DISCLAIMER

Issued by Sandia National Laboratories, operated for the United States Department of Energy by Sandia Corporation.

Printed in the United States of America

Available from
National Technical Information Service
U. S. Department of Commerce
5285 Port Royal Road
Springfield, VA 22161

NTIS price codes
Printed copy: $6.00
Microfiche copy: A01

PAGES 1 to 2

WERE INTENTIONALLY

LEFT BLANK

0769
SAND80-~~0679~~
Unlimited Release
Printed July 1980

Distribution Category
UC-70

SAND--80-0769

M80005954

THERMAL CONDUCTIVITY OF SILICIC TUFFS: PREDICTIVE FORMALISM AND COMPARISON WITH PRELIMINARY EXPERIMENTAL RESULTS

Allen R. Lappin
Geological Projects Division 4537
Sandia Laboratories
Albuquerque, NM 87185

ABSTRACT

Performance of both near- and far-field thermomechanical calculations to assess the feasibility of waste disposal in silicic tuffs requires a formalism for predicting thermal conductivity of a broad range of tuffs. This report summarizes the available thermal conductivity data for silicate phases that occur in tuffs and describes several grain-density and conductivity trends which may be expected to result from post-emplacement alteration. A bounding curve is drawn that predicts the minimum theoretical matrix (zero-porosity) conductivity for most tuffs as a function of grain density. Comparison of experimental results with this curve shows that experimental conductivities are consistently lower at any given grain density. Use of the lowered bounding curve and an effective gas conductivity of 0.12 W/m°C allows conservative prediction of conductivity for a broad range of tuff types. For the samples measured here, use of the predictive curve allows estimation of conductivity to within 15% or better, with one exception. Application and possible improvement of the formalism are also discussed.

CONTENTS

ILLUSTRATIONS

ILLUSTRATIONS (Cont)

TABLES

THERMAL CONDUCTIVITY OF SILICIC TUFFS: PREDICTIVE FORMALISM AND COMPARISON WITH PRELIMINARY EXPERIMENTAL RESULTS

Introduction and Objectives

As a result of both modeling studies and attempts to evaluate tuffs as a disposal medium for heat-producing wastes, it has become apparent that a formalism for prediction of tuff thermal conductivity is sorely needed. This report describes and develops such a predictive formalism.

Specific objectives of this study were to

1. Describe and tabulate the available thermal conductivity data for the silicate phases occurring in silicic tuffs
2. Provide estimates of the theoretical (zero-porosity) matrix conductivity of silicic tuffs as a function of grain density, and hence of both mineralogy and postemplacement alteration processes
3. Compare calculated zero-porosity matrix conductivities extrapolated from laboratory measurements with the theoretical curves
4. Develop predictive curves for tuff matrix conductivity, based on the comparison made in 3
5. Evaluate the accuracy of the predictive formalism when applied to both natural-state and dehydrated tuffs
6. Compile the available data on tuff thermal conductivity, both at ambient conditions and at elevated temperatures and pressures.

Thermal Conductivity of Major Silicate Phases in Silicic Tuffs

Silicic tuffs contain varying proportions of silicic glass, silica polymorphs, feldspars, zeolites, and clays, plus generally minor amounts of metal oxides and mafic silicates.[1-3] This section summarizes the available information on thermal conductivity of the major silicate phases in tuffs.

Natural silicic glass, roughly similar to granite in composition, makes up a large part of most unaltered silicic tuffs. Fresh glasses usually contain only a few tenths of a weight percent water,[4] which is entrained at magmatic temperatures. Interaction with either deuteric water or ground waters, however, results in significant hydration of the glasses in most glassy tuffs.[5] Glass water contents of up to 7 wt % or more are not uncommon.[6]

Data on the ambient-temperature thermal conductivity of natural glasses are very limited (see Table 1). Of the available values, that given by Murase and McBirney[7] (K = 1.26 W/m°C) is for a rhyolite obsidian containing 0.5 wt % water. The water content of the obsidian studied by Birch and Clark[8] (K = 1.42 W/m°C) is not specified. Comparison of the reported obsidian conductivities with that of fused silica (1.33 ± 0.04[9]) and of basaltic glass (1.37 W/m°C[8]) is consistent with the assumption that the ambient-temperature thermal conductivity of anhydrous silicic glass is largely insensitive to glass composition, with an average value near 1.35 W/m°C. Effects of varying water content are unknown; increasing hydration presumably decreases glass conductivity toward a minimum value greater than that of liquid water (0.6 W/m°C).

Virtually no tuff is free of phenocrysts, which are relatively coarse crystals entrained at the time of eruption. Two types of phenocrysts are of major interest here. In many tuffs, the major phenocryst is feldspar.[3] In some cases, zoned plagioclase feldspars are present and may cover a broad range in composition. The thermal conductivity of plagioclase, as shown in Table 1 and Figure 1, is a marked function of composition.[10] As the composition ranges from $Ab_{100}An_0$ (albite-$NaAlSi_3O_8$) to Ab_0An_{100}

(anorthite-$CaAl_2Si_2O_8$), the thermal conductivity decreases from 2.3 W/m°C to a minimum (~1.5 W/m°C) at about $Ab_{50}An_{50}$ and then increases to 1.7 W/m°C. The zonation of plagioclases in most tuffs is "normal"; i.e., with more sodic plagioclase toward the margins of the phenocryst. Representative plagioclase compositions of tuffs from the Yucca Mountain area of NTS range from $Ab_{60}An_{40}$ to $Ab_{90}An_{10}$.[2 11] Plagioclase phenocrysts generally make up 10 vol % or less of these tuffs.

Table 1

Thermal Conductivities and Grain Densities of Silicate Phases in Silicic Tuffs

Phase	Grain Density (g/cm^3)	Thermal Conductivity (W/m°C)
Obsidian	2.41[15]	1.42[8]
		1.26[7]
Fused Silica	2.205	1.36
		1.33±0.04[9]
Basaltic Glass	-	1.37[8]
Quartz	2.647	
Parallel to c		11.60±0.58[8]
Perpendicular to c		6.84±0.34[8]
Geometric Average		7.69
-Cristobalite	2.334	6.15[13]
Feldspars		
Plagioclase (Ab = $NaAlSi_3O_8$; An = $CaAl_2Si_2O_8$)		
$Ab_{99}An_1$	2.606	2.32
$Ab_{96}An_4$	2.629	2.35
$Ab_{94}An_6$	2.631	1.94
$Ab_{92}An_8$	2.607	1.97
$Ab_{89}An_{11}$	2.642	1.98
$Ab_{46}An_{54}$	2.701	1.53
$Ab_{27}An_{73}$	2.703	1.47
$Ab_{22}An_{78}$	2.700	1.67
$Ab_{20}An_{80}$	2.730	1.54

Table 1 (Cont)

Phase	Grain Density (g/cm^3)	Thermal Conductivity (W/m°C)
$Ab_{04}An_{96}$	2.769	1.68
Potassium Feldspars ($KAlSi_3O_8$)		
Sanidine	2.573	1.65
Orthoclase	2.583	2.32
Microcline	2.560	2.49
Zeolites		
Analcime	2.254	1.27
Natrolite*	2.239	2.00
Chabazite	2.139	1.22
Stilbite*	2.170	1.18
Layer Silicates		
Biotite	2.89 to 3.08	2.34 to 1.70
Muscovite	2.83 to 2.87	2.50 to 2.21
"Mixed-Layer" and Montmorillonite		
Fully Collapsed†	2.83 to 3.08	2.50 to 1.70
Fully Expanded (Mont.)	2.20 to 2.36	1.55 to 1.20
Hornblende	3.11 to 3.25	3.08 to 2.54
Augite	3.275	3.82
Calcite	2.721	3.59
Chlorite	2.64 to 2.86	4.35 to 6.18
Epidote	3.16 to 3.40	3.04 to 2.63

*Not reported in tuffs at NTS; included to increase coverage of zeolites.

†Conductivity values calculated, assuming that interlayer water of expandable clays produces spacing of 15 Å and has the same conductivity as that of liquid water.

(Unless specifically noted otherwise, all data are from Reference 10.)

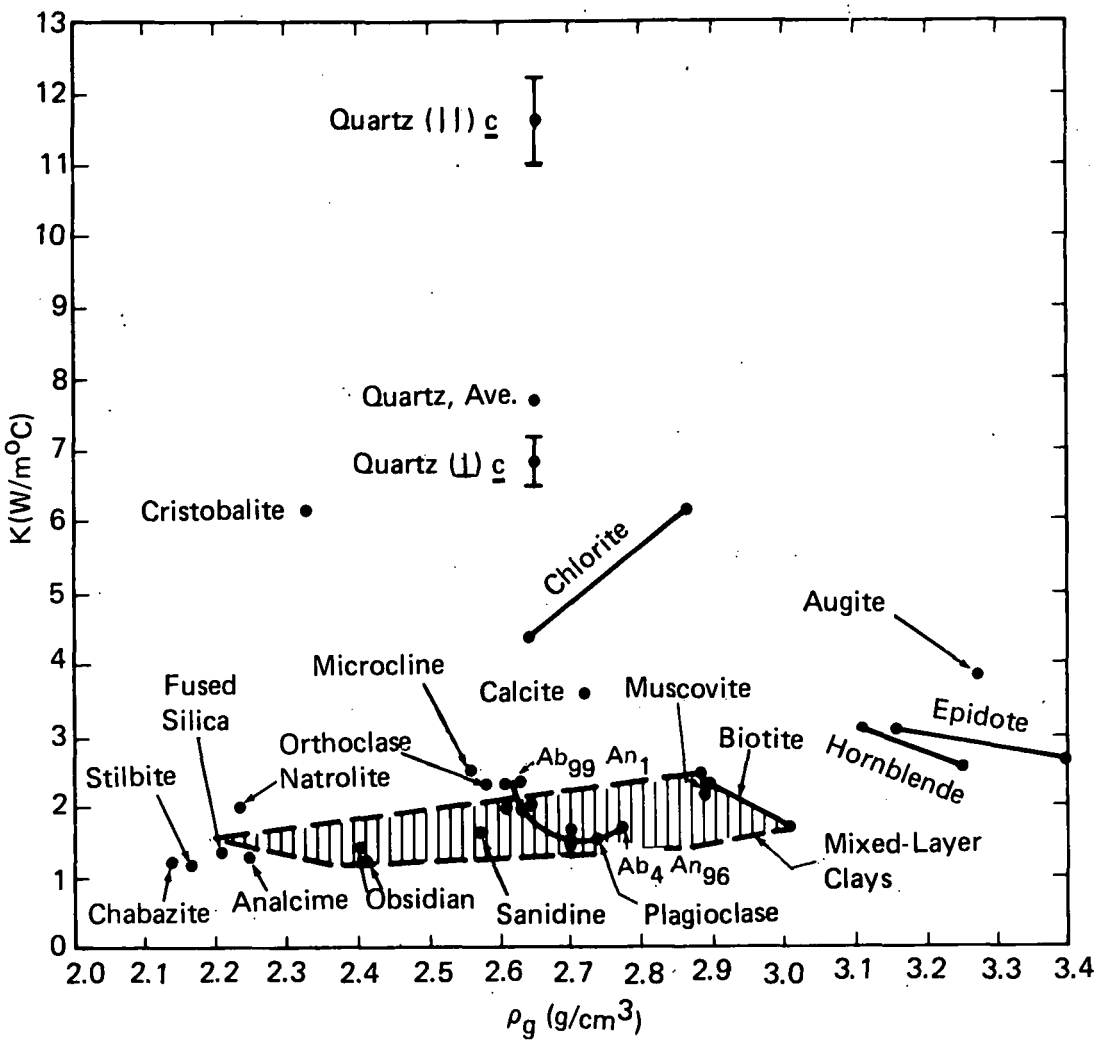

Figure 1. Thermal Conductivity Versus Grain Density for Silicate Phases in Silicic Tuffs

A second feldspar, sanidine or anorthoclase, also commonly occurs as phenocrysts in silicic tuffs. Sanidine, a high-temperature potassium feldspar ($KAlSi_3O_8$), has a reported thermal conductivity of 1.65 W/m°C,[10] and makes up as much as 15 vol % of the tuffs at Nevada Test Site (NTS).[3] Anorthoclase, a high-temperature ternary feldspar--a mix of albite ($NaAlSi_3O_8$), sanidine ($KAlSi_3O_8$) and anorthite ($CaAl_2Si_2O_8$) molecules, with anorthite the least abundant--also occurs as phenocrysts in tuff, but no thermal conductivity data for this phase are available.

Quartz is the second type of phenocryst common in silicic tuffs, though it is generally less abundant than feldspar. It also occurs as an authigenic mineral in some deeply buried tuffs. Abundant ambient-temperature thermal conductivity data exist for quartz, as summarized in Reference 9 and indicated in Table 1 and Figure 1. The thermal conductivity of quartz is a strong function of the direction of heat flow relative to the crystallographic axes. This could result in a strong conductivity anisotropy in rocks where the quartz is relatively abundant and had a strongly preferred orientation. In rocks where this is not the case, the nondirectional or "average" value of 7.69 W/m°C[10] can be used. Since the conductivity of quartz is much higher than that of other silicates in tuffs, overall tuff conductivity will be strongly sensitive to quartz content.

Primary mafic silicates such as biotite, hornblende, and pyroxene are common in tuffs but generally sum to less than 5 vol % of the total rock, at least in the case of tuffs associated with the Timber Mountain Caldera on and near NTS.[3] Their reported conductivity values are included in Table 1 and shown in Figure 1.

Many welded tuffs devitrify soon after emplacement. In this process the original or hydrated glass crystallizes to a mixture of silica polymorphs and alkali feldspars. Because of the heat present, devitrification of welded tuffs may be nearly contemporaneous with welding and involve little hydration. In nonwelded tuffs the process is much slower since it occurs at near-ambient temperatures, and is often more complex, generally involving extensive glass hydration and perhaps other mineralogical reactions as well. At this point, only devitrification that occurs in welded tuffs is considered. The silica polymorph generally resulting from devitrification is cristobalite,[1 12] except in very slowly cooled units or peralkaline ash flows, where quartz is frequently formed. Only devitrification to cristobalite is considered at this point. The one available reported conductivity value of cristobalite (6.15 W/m°C[13]) is given in Table 1 and indicated in Figure 1. No information concerning directional dependence of conductivity in cristobalite is available.

Little is known about the detailed feldspar mineralogy of the ground mass in devitrified tuffs because of the very fine-grained nature of the feldspar-cristobalite intergrowths, i.e., the individual crystals are only a few micrometres in size. The groundmass feldspar is generally reported only as "alkali feldspar." Recent analyses,[2 11] indicate that in a wide range of devitrified tuffs, the groundmass feldspar is intermediate in composition between pure orthoclase ($KAlSi_3O_8$) and albite ($NaAlSi_3O_8$), with an average composition near $Or_{60}Ab_{40}$. The lack of twinning suggests that the feldspar is effectively monoclinic (ortho-clase or sanidine) rather than triclinic (microcline). If the groundmass feldspar is still in the high-temperature (sanidine) structural state, its ambient-temperature conductivity should be near 1.95 W/m°C. If it is in the orthoclase structural state, then the ambient-temperature conductivity may be very near 2.32 W/m°C regardless of composition since orthoclase and albite have very similar conductivities. This is true unless a decrease in conduc-tivity due to mixing of Na, K end members occurs as in the case of Na, Ca plagioclase feldspar end members.

Another type of alteration of tuffs involves interaction with ground-water, or possibly deuteric water, and resulting formation of zeolites and/or clays. These phases are relatively more abundant in tuffs that have spent much time below the water table,[6] although tuffs well above the water table have also been shown to undergo complex alteration processes in some situations.[14] Thermal conductivity data pertaining to zeolites are limited to the four values shown in Table 1. Of the four minerals listed, only analcime (1.27 W/m°C) and chabazite (1.22 W/m°C) are reported to occur in silicic tuffs. Zeolites reported in the tuffs at NTS include clinoptilolite (which predominates), heulandite, analcime, chabazite, erionite, mordenite, and phillipsite.[2 6 11] The grain densities of these minerals, all hydrated framework aluminosilicates, range from a low of 2.02 (erionite) to 2.25 g/cm^3 (analcime).[15] Clinoptilolite, the most common zeolite in silicic tuffs, has a density of 2.16 g/cm^3. Conduc-tivity within the zeolite group may obviously vary widely.

Thermal conductivity data for layer silicates other than micas also appear lacking. Reported values for biotite (1.70 to 2.34 W/m°C) and

muscovite (2.21 to 2.50 W/m°C) are included in Table 1. Clays occurring in silicic tuffs as a result of alteration are generally illites (very similar to muscovite in composition), mixed-layer illite-montmorillonites, or montmorillonites.[6 14 16] Since no conductivity data exist for montmorillonites and mixed-layer clays, they have been estimated in Table 1. It has been assumed that the conductivity of the lattice portion of interlayered clays ranges from that of muscovite to that of Fe-rich biotite, that the fully expanded montmorillonites have a basal spacing of 15 Å, and that the water in the expanded layers (though in fact partly structured) has the thermal conductivity of liquid water. Conductivity ranges shown for the interlayered clays and montmorillonites were calculated by using the geometric-means method described in the next major section of this report. Depending upon the extent of interlayering and composition, the conductivity of an interlayered clay could vary anywhere within the indicated bounds.

If waste is emplaced in tuffs so as to result in significantly increased temperatures, the thermal conductivity of the tuff emplacement medium at elevated temperatures will need to be well understood. Accordingly, presently available relevant data are discussed here.

Thermal conductivities of the glasses listed in Table 1 all increase with increasing temperature, as shown in Figure 2. Averaging the data for the two rhyolite obsidians and fused silica yields an increase in glass conductivity of about 0.001 W/m°C per degree centigrade. Thus, for an assumed ambient-temperature glass conductivity of 1.35 W/m°C, a 135°C temperature rise would be required for the glass conductivity to increase by 10%.

Available data for thermal conductivity of feldspars as a function of temperature[8] indicate that this factor probably need not be considered. As shown in Figure 2, the conductivity of sodic oligoclase (An_{12}) decreases very slightly with increasing temperature, while that of more calcic plagioclases (An_{60} and An_{80}) increases slightly. In no case measured, however, does the conductivity of plagioclase change by as much as 10% between ambient temperature and 200°C. It is assumed below that

the conductivity of both glasses and feldspars is not sensitive to temperature.

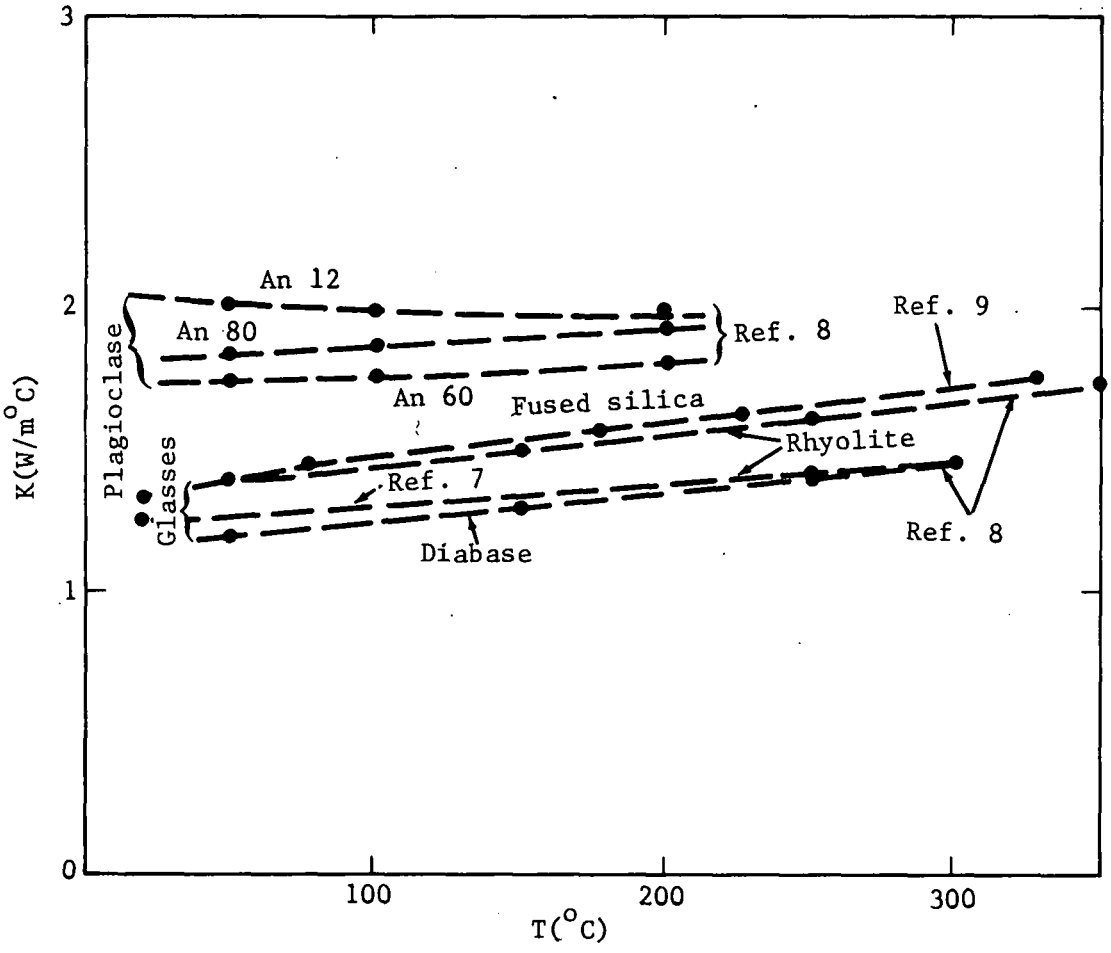

Figure 2. Thermal Conductivities of Glasses and Feldspars as a Function of Temperature

This is not the case for quartz, as shown in Figure 3. Measured conductivity values for quartz decrease by as much as 40% between 20 and 200°C. A conductivity decrease of 10% occurs between 20 and 50°C. No data are available describing the sensitivity of conductivity to temperature in the cases of cristobalite, zeolites, or the other additional phases indicated in Figure 1 and Table 1.

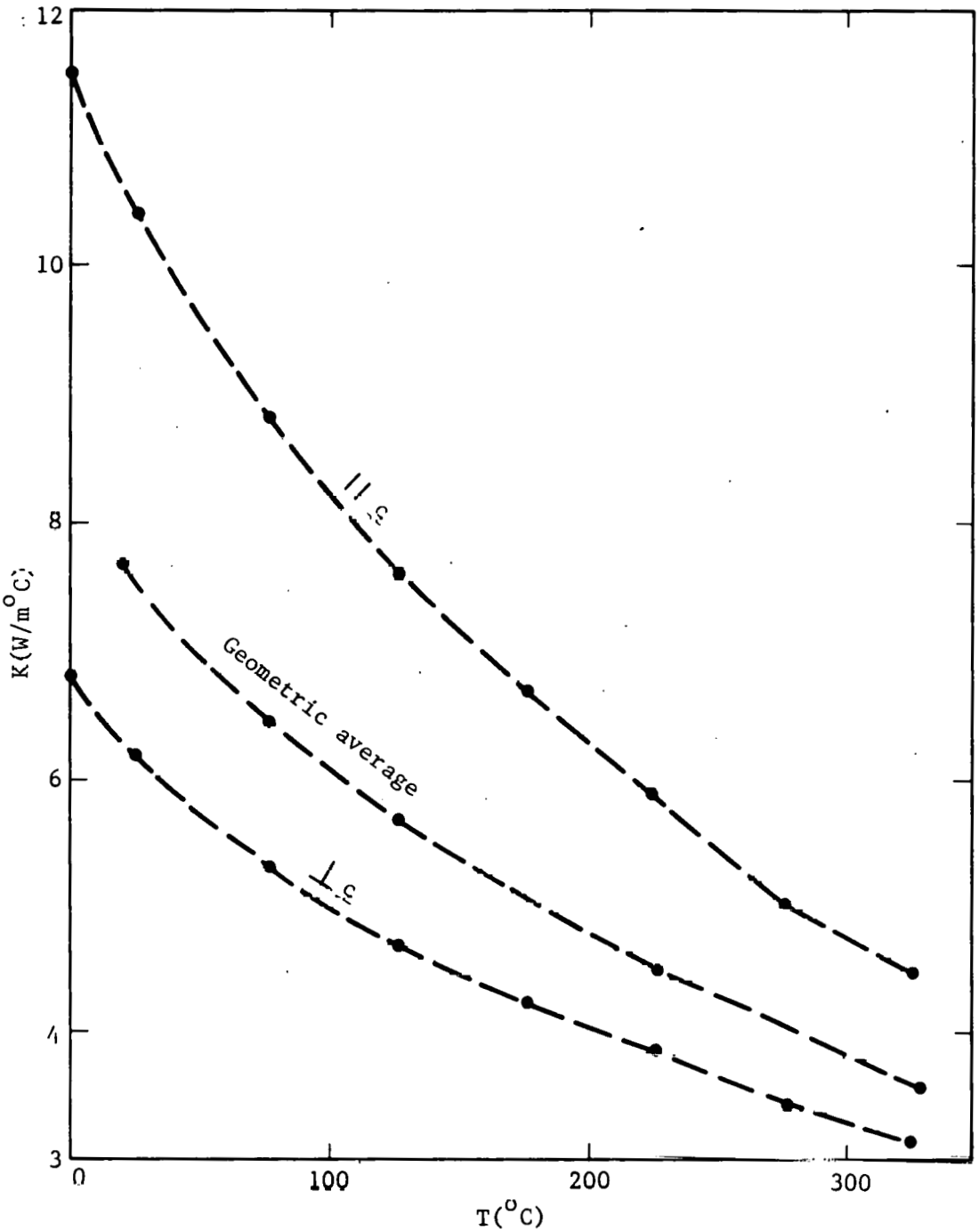

Figure 3. Thermal Conductivity of Quartz as a Function of Orientation and Temperature

Theoretical Matrix Conductivity of Tuffs

The previous section discussed the thermal conductivity of major phases occurring in silicic tuffs. This section describes the application of these data to estimation of the zero-porosity or theoretical matrix conductivity of tuffs. Also discussed are several assumptions and limitations necessary and inherent in this estimation.

Several attempts have been made to calculate the zero-porosity thermal conductivity of rocks from an estimate of their mineralogical makeup. Perhaps the most thorough is that of Robertson and Peck,[17] who discuss several calculational procedures that can be used to estimate the zero-porosity conductivity of basalts and to compare calculated results with values measured on fine powders.

One method is to assume that the average of conductivity values calculated by assuming heat flow (formally equivalent to flow of electric current) in parallel and in series represents the conductivity of the rock matrix. Use of this approach by Robertson and Peck yielded a calculated matrix conductivity 2.57 W/m°C for basalt, versus a measured value of 2.55 W/m°C. Use of a quadratic formalism, again assuming a random fabric and averaging values calculated for parallel and series flow, yielded a calculated conductivity identical to the measured value of 2.55 W/m°C.[17] Both of these methods are based on analogs to electrical conductivity theory, but are cumbersome to calculate.

A third method, the weighted geometric mean method,[18] also yielded a theoretical matrix conductivity of basalt equal to the measured value at zero porosity. This formalism is strictly empirical, but is easy to use in making calculations, and can explicitly treat variable states of rock saturation. The conductivity of a mineral aggregate is calculated according to this method from the relation

$$K_a = K_1^{x1} K_2^{x2} \ldots K_n^{xn} \qquad (1)$$

where

K_a = conductivity of aggregate

K_1 .. K_n = conductivities of the individual phases

x1 .. xn = volume fractions of the individual phases

In order to use this formalism for prediction of tuff conductivities, however, some generalizations about the thermal conductivity of the different groups of silicates present must be made.

As mentioned above, data on the thermal conductivity of natural glasses and zeolites are limited. Therefore, it is assumed here that the conductivity of all glasses in tuffs is the same (about 1.35 W/m°C) and that the conductivity of all zeolites is 1.25 W/m°C. Possible effects of glass hydration are specifically ignored.

Virtually all tuffs contain some phenocrysts, whose potential effects must be considered. Accordingly, a series of calculations was made to estimate the changes in matrix conductivity of glassy tuffs as a function of quartz, sanidine, and plagioclase (An_{30}) content. For an assumed glass conductivity of 1.35 W/m°C, contents of up to 25% sanidine and plagioclase change the theoretical matrix conductivity by less than 10%; calculated values are 1.42 and 1.40 W/m°C, respectively. Only 5% quartz is required however, to change the matrix conductivity by nearly 10%, from 1.35 to 1.47 W/m°C. Ideally, then, the quartz phenocryst content of tuffs should be considered before estimation of the matrix conductivity. Since in virtually all tuffs treated here the quartz content is well below 5%,[2 3 11] the presence of quartz phenocrysts is ignored. Mafic phenocrysts are also assumed negligible.

The case is more complicated for tuffs devitrified solely to a mix of cristobalite and feldspar. The volumetric cristobalite/feldspar ratio in the groundmass of such tuffs probably ranges from 30/70 to 40/60, based on the general compositional similarity to granite. Two specific examples calculated for the calcalkaline Topopah Springs and peralkaline Grouse

Canyon tuffs and based on compositions given in Reference 5, are 40/60 and 31/69, respectively. If the groundmass feldspar is assumed to have a conductivity of 2.32 W/m°C (orthoclase), variation from 30 to 40% cristobalite content results in a range of calculated matrix conductivity (assuming no other phases are present) of between 3.11 and 3.43 W/m°C. The assumed average rock (35/65) would have a matrix conductivity of 3.26 W/m°C and a grain density of 2.503 g/cm^3. If, however, the groundmass feldspar in a given tuff (35/65 cristobalite/feldspar) is sanidine rather than orthoclase, the matrix conductivity decreases to 2.61 W/m°C, and grain density to 2.487 g/cm^3. Occurrence of quartz in devitrified tuffs would increase conductivity.

Devitrification is not, however, the only high-temperature process involving the formation of silica polymorphs and feldspars in tuffs. A closely related process, vapor-phase crystallization, also frequently occurs.[12] In this process, vapors given off by the compacting and cooling tuff unit deposit silica polymorphs (tridymite and/or cristobalite) and alkali feldspars generally as void fillings in the porous upper portions of a welded unit or as replacement of pumice fragments. The products of vapor-phase crystallization are generally distinguishable in thin section from the products of devitrification by their coarser grain size and location. In the absence of data on the thermal conductivity of tridymite, it is assumed here that the thermal conductivity of vapor-phase minerals is the same as that of devitrification products.

In many cases, devitrification appears to be quite uniform and complete, especially in thick welded and ash-flow tuffs well above the water table. For example, of the 330 m of the Topopah Springs Member of the Paintbrush Tuff encountered in Hole Ue25A#1 on NTS, some 290 m, although completely devitrified, appear to have undergone limited alteration other than this.[11 16 19] The nonwelded margin and quartz latite caprock at the top of the unit are still vitric and are some 7 m thick. The poorly welded envelope and basal vitrophyre at the base of the tuff are also still largely vitric and are about 31 m thick. The devitrified central portion of the Topopah Springs appears to be some 290 m thick, for which the zero-porosity matrix conductivity should be fairly

uniform, but should reflect the well-documented compositional changes occurring vertically throughout.[19] In addition, in some portions of the unit, cristobalite resulting from devitrification has at least partially inverted to quartz.

Deep-seated tuffs, especially those below the water table for extended periods of time, also frequently display inversion of cristobalite formed during devitrification. Generally some coarsening of the texture also occurs in this process. An excellent example is seen in the Bullfrog Member of the Crater Flat Tuff in Holes J-13 and Ue25A#1 on NTS.[2 11] If this process proceeds to completion, the increased conductivity of quartz relative to cristobalite should result in a zero-porosity matrix conductivity of 3.53 W/m°C (assuming 35 vol % total quartz) as compared to 3.26 W/m°C for an equivalent devitrified tuff free of quartz. The grain density of this tuff would ideally be 2.616 g/cm^3.

Figure 4 shows the general trends of theoretical matrix conductivity in tuffs as a function of mineralogy, and hence alteration processes. Assume that a tuff is extruded as a thick ash-flow unit and initially consists entirely of glass with a conductivity of 1.35 W/m°C (Point I in Figure 4). If the tuff is hot enough and thick enough at the time of emplacement, massive devitrification to cristobalite and feldspars will occur along Trend A, with correlative increases in both grain density and conductivity. Variations in the conductivity of the devitrified material (Curve II) reflect variations in tuff composition. Inversion of cristobalite to quartz within a devitrified tuff should drive the matrix conductivity along Trend B toward a curve representing variations in conductivity of quartz-feldspar aggregates as a function of quartz content (Curve III). Though some alteration of the initial glass composition by hydration before devitrification may occur,[5] the two processes described thus far are largely isochemical.

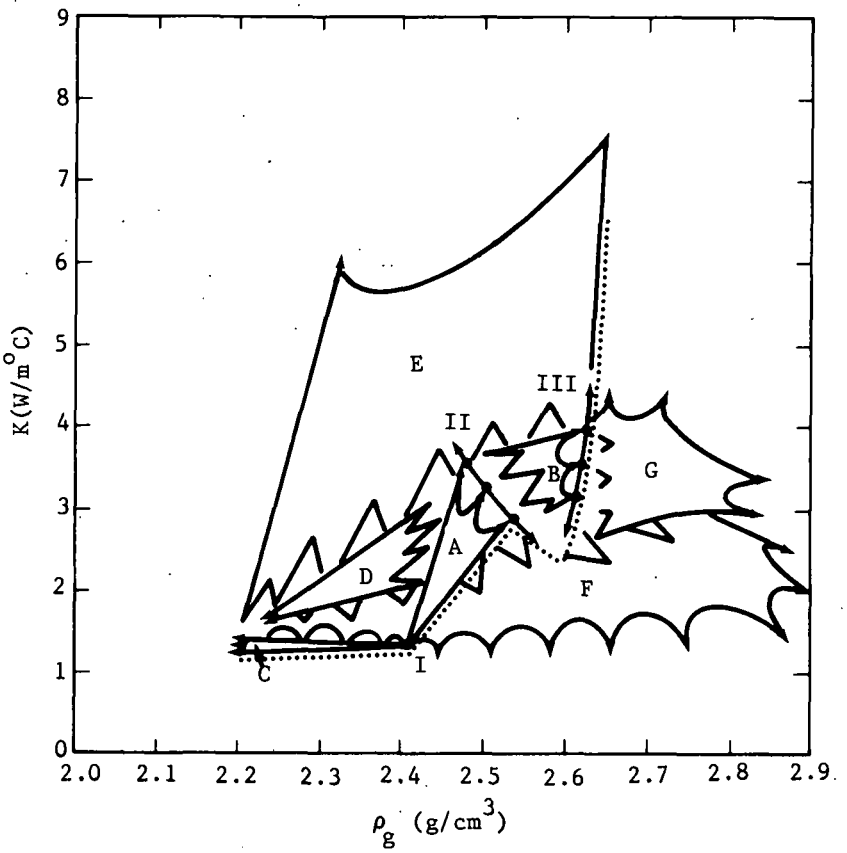

Point I: Assumed conductivity and grain density of primary silicic glass

Trend A: Devitrification to cristobalite plus feldspars

Curve II: Uncertainties in conductivity of simply devitrified tuff as function of variable cristobalite/feldspar. Specific points shown (with increasing conductivity are 25/75, 35/65, 45/55

Trend B: Partial to complete inversion of cristobalite to quartz in devitrified tuffs

Curve III: Uncertainties in conductivity of quartz-bearing tuffs as function of variable quartz/feldspars. Specific points shown (with increasing conductivity) are 25/75, 35/65, and 45/55

Trend C: Zeolitization of initially vitric tuff

Trend D: Zeolitization of devitrified tuff

Trend E: Silicification of zeolitized to quartz-rich tuffs. End points are cristobalite (low-density) and quartz

Trend F: Argillic alteration

Trend G: Propylitic alteration

Dotted line: Minimum bounding curve for tuffs that are either still vitric or have undergone alteration processes A to E

Figure 4. Theoretical Trends in Matrix Thermal Conductivity as Functions of Grain Density and Mineralogy

Replacement of primary glass by zeolites (Trend C) should have little effect on the zero-porosity conductivity of vitric tuffs, since the conductivity of zeolites (1.2 to 1.3 W/m°C) is similar to that of the glass (1.35 W/m°C). This would also be true for zeolite precipitation in the pore spaces of a vitric tuff, since the porosity does not enter into the zero-porosity conductivity as figured here. Deposition of zeolites within the pore space of devitrified tuffs, however, could greatly affect the matrix conductivity (Trend D), because of the large difference between the conductivity of the devitrification products (~3.2 W/m°C) and the zeolites (1.2 to 1.3 W/m°C).

While much information is available on the distribution of zeolite zonation or occurrences in zeolite-bearing rocks (see, for example, References 2, 6, and 20), there appears to be little information on the uniformity of degree of zeolitization in a given area of tuffs. In fact, the available information concerning zeolitization of the tuffs near Yucca Mountain at NTS[2 11 16] indicates that the extent of alteration, even in the same tuff units, may vary over fairly short distances both vertically and horizontally. This variability must be well understood before the limits to accuracy of thermomechanical modeling can be determined.

Silicification (Trend E) is a process by which silica minerals, either cristobalite or quartz, are deposited in tuffs as a result of interaction with silica-saturated groundwaters. It is a common alteration process[16] and should always lead to increases in the theoretical matrix conductivity because of the high thermal conductivity of both quartz and cristobalite.

Argillization (Trend F) is a process by which clay minerals, largely mixed-layers clays and montmorillonites, are formed. This may occur in either glassy tuffs[14] or by prolonged reactions with and leaching of devitrified or quartz-bearing tuffs. As shown in Figure 4, argillization of glassy or highly zeolitic tuffs should have little effect on matrix conductivity. The matrix conductivity of either cristobalite- or quartz-bearing (microgranitic) tuffs should be greatly decreased by argillization. Because of the large uncertainties in extent of mixed layering,

however, the direction or trend along which this decrease occurs is undefinable in detail. The very broad front of Trend F reflects this uncertainty, since it must include conductivities ranging all the way from that of nonexpandable clays (muscovite and Fe-biotite) to estimated conductivities of fully expanded montmorillonites.

Propylitic alteration is a process (Trend G) by which one or more of the minerals calcite, chlorite, and/or epidote are formed in tuffs. This type of alteration occurs at several localities in southern Nevada.[21] Regardless of the detailed mineralogy of the alteration, it would appear to lead to increased grain density of the altered tuffs. During chloritic alteration, matrix conductivity would generally increase. As shown (see also Figure 1), growth of calcite and/or epidote might have little effect on matrix conductivity, but would increase grain density. In the process of alunitization, alunite ($KAl_3(OH)_6(SO_4)_2$) is deposited in tuffs. No thermal data are available for alunite, and the process is not considered further here.

In Figure 4, a dotted line has been drawn below the expected variations in conductivity resulting from Trends A through E described above. This curve would appear to estimate the minimum theoretical matrix conductivities of most silicic tuffs as a function of grain density (directly) and mineralogy (indirectly). Tuffs reflecting processes A, completion of B, C, and part of E should lie near the line. The matrix conductivities of tuffs reflecting partial completion of B, any part of D, and the bulk of E, should lie above it. Theoretical matrix conductivities of tuffs that have undergone significant argillic or propylitic alteration are not treated or considered by the bounding curve.

Effective Matrix Conductivity of Tuffs

To be of any usefulness, a predictive scheme describing the thermal conductivity of tuffs must account for the effects of porosity and, if tuffs above the water table are to be considered, for the degree of saturation. This is especially true since tuffs vary so widely in

porosity (from near 0 to 50% or more) and may contain more than one kind of porosity, and since the details of porosity geometry and distribution in tuffs are unknown at present.

For tuffs, individual pores cannot be expected to be uniform in shape and distribution. In vitric tuffs matrix porosity will consist largely of the void spaces between individual glass shards. Thus, pores will be spherical or nearly so in totally nonwelded tuffs but will be increasingly deformed as a tuff is welded or compacted. In the extreme, it may be expected that the pores remaining in a densely welded vitric tuff will be largely planar and occur at the boundaries between the highly compressed shards. In such a rock, the cross-sectional porosity measured in a section cut perpendicular to layering may be significantly less than that in a section parallel to layering. Thus, it is to be expected that the thermal conductivity of welded vitric tuffs will be greater parallel to layering than perpendicular to it.

In the case of devitrified tuffs, the intergranular porosity should be distributed differently. In general, the devitrification fabric grows at right angles to the preexisting shard fabric (see figures in Reference 1) with the result that grain boundaries are elongated perpendicular to layering. As a result of this reorientation of the rock fabric, the matrix thermal conductivity of devitrified welded tuffs will probably be somewhat greater perpendicular to layering than parallel to it. The extent of this effect is not now evident. Fabric-related variations considered here do not include possible effects of zeolitization or silicification.

Two additional factors complicate an understanding of the effects of porosity on tuff conductivity. First, part of a tuff's porosity is often in the form of relatively porous pumice fragments entrained at the time of eruption. These fragments may be 5 cm or more in diameter, often resist welding relative to the matrix as a whole, and may be corroded or dissolved as a result of vapor-phase reactions and deposition.[12] Such pumice fragments occasionally cause trouble in the measurement of thermal conductivity on relatively small samples, especially by the transient line

source method, since they result in too low an apparent thermal conductivity if immediately next to the heat source. In the samples analyzed here, porosity measurements were made on coherent matrix material. Thus the reported values average out the effects of some pumice fragments and may be either too low or too high for the small region of the sample in which the conductivity was actually measured. A second type of irregular porosity, lithophysae, is also present in some tuffs. These subspherical cavities, often 3 cm or more in diameter, form in thick tuffs as a result of gas evolution. For example, Hole UE25A#1 encountered two lithophysal zones totaling some 70 m in thickness in the Topopah Springs Member of the Paintbrush Tuff.[16] It has not yet been possible to make any conductivity measurements on lithophysal tuff. Certainly the presence of lithophysae may be expected to lower the in-situ conductivity of a given tuff relative to that expected on the basis of general matrix porosity alone.

With these provisos in mind, however, a simple extension of the geometric means approach of Woodside and Messmer,[18] is used here to estimate tuff thermal conductivity as a function of theoretical matrix conductivity (K_o), porosity, and degree of saturation. The formalism used is shown by

$$K_{rock}^{meas} = K_o^{(1-\phi)} K_g^{\phi(1-s)} K_w^{\phi s} \quad , \tag{2}$$

where

K_{rock}^{meas} = measured rock conductivity

K_o = theoretical matrix conductivity

ϕ = porosity

K_g = conductivity of air

s = relative saturation of sample

K_w = conductivity of liquid water

By means of simple rearrangement, <u>calculated</u> K_o values can be obtained from

$$K_o = \left(\frac{K_{rock}^{meas}}{K_g^{\phi(1-s)} K_w^{\phi s}} \right)^{\frac{1}{1-\phi}} \qquad (3)$$

It is only by use of these K_o values that the extent of agreement between theory and measured tuff matrix conductivities can be evaluated. In these calculations, Equation 3, the measured conductivity and calculated saturation of the natural-state sample are generally used. K_o is assumed independent of direction of heat transfer and rock fabric. It is assumed that ϕ, the porosity (calculated from $\phi = 1 - \rho_{db}/\rho_g$ where ρ_{db} is the dry-bulk density and ρ_g is grain density after heating to 110°C) is uniformly distributed throughout the rock. Thus, the distinction between effective (connected) and total porosity is ignored, as are any variations in the actual shape or size of different kinds of pores present. It is further assumed initially that the thermal transfer across gas-filled porosity in a partially saturated or completely dehydrated sample is limited by the thermal conductivity of air or steam, K_g, at all temperatures. That is, radiative transfer and convection across and within pores can be ignored. It is also assumed that the thermal conductivity of pure water, K_w, is the conductivity for the liquid-filled portion of the porosity; i.e., the ion content of the pore water is low enough not to have any appreciable effect. Finally, it is assumed in Equations (2) and (3) that the calculated degree of saturation of a sample is uniform throughout.

The validity of Equations (2) and (3) depends not only on the validity of assumptions discussed above but also on the ability to determine K_{rock}^{meas} and bulk material properties accurately. This is especially true for the grain density (ρ_g), porosity (ϕ), and degree of saturation(s).

Grain density can, under most conditions, be measured quite accurately, probably to much better than ± 0.01 g/cm^3. Two factors may decrease this level of accuracy. In the analytical procedure used, grain densities were measured after heating of samples to about 110°C until all

evolution of volatiles ceased. Thus, in samples containing appreciable amounts of expandable clays, zeolites, and/or hydrated silicic glass, alteration of constituent grains from their natural-state grain density might result. Actual measurement of grain volume, however, was done by water pycnometer. Thus, partial rehydration of some minerals might occur during measurement. Dehydration of expandable clays would give too low an apparent weight of dried sample, as would dehydration of zeolites. Rehydration of expandable clay should yield a measured displacement slightly larger than the real volume, while rehydration of zeolites should yield a measured displacement slightly less than the true volume. Thus, possible effects on expandable clays during sample preparation should lead to too low a grain density, while dehydration of zeolites would have an undetermined effect.

Porosity values used in this report are calculated from the relation $\phi = (\rho_g - \rho_{db})/\rho_g$, where ρ_g and ρ_{db} are the sample grain and dry-bulk densities. Saturation values are calculated from the relationship

$$s = \left(\frac{\rho_b - \rho_{db}}{\phi}\right) = \frac{\left(\rho_b - \rho_{db}\right)\rho_g}{\left(\rho_g - \rho_{db}\right)} \quad ,$$

and are hence affected directly by uncertainties in bulk, dry-bulk, and grain densities.

Some effects of uncertainties in these variables are considered indirectly in Figure 5, in which K_{rock}^{calc} is plotted as a function of porosity and degree of saturation. Three trends shown by Figure 5 are worth brief discussion. For fully saturated rocks, the decrease in conductivity with increasing porosity is fairly linear. However, the relative decrease increases with increasing porosity, since the absolute conductivity decreases. Thus, measurements of both grain density and dry-bulk density, and resultant calculated porosities, are most critical in high-porosity materials, i.e., in those materials where the calculations should be most accurate. Unfortunately, it is these tuffs that generally also have the highest contents of zeolites, hydrated glass, and clays. Sensitivity of

conductivity to uncertainty in degree of saturation increases in both the relative and absolute sense with increasing porosity as well. Again, however, barring mineralogical effects, calculated saturations should be most accurate for high-porosity material. Finally, both absolute and relative errors in estimated conductivity resulting from uncertainties in porosity are greater for dehydrated tuffs (s = 0) than for saturated tuffs, due to the low thermal conductivity of air.

As shown by Equation (3), values of K_o calculated from data on samples for which the conductivity has been measured are strongly sensitive to the measured rock conductivity, K_{rock}^{meas}. All conductivities reported here were measured by the transient line source technique,[22] which involves axial emplacement of a high-aspect ratio (large length/diameter) heat source within a sample, and the monitoring of the temperature rise at the center of the heated zone as a function of time at an accurately known power output per unit length of heat probe. In the data reduction scheme, radial symmetry of conductivity around the line source is assumed. Experimentally, the major uncertainties appear to lie in possible alteration of sample state during sample preparation, contact resistance between the heat probe and rock, uncertainties in power output and measurement of heat-probe temperature, and unexpected sample inhomogeneities near the central portion of the heat probe where the thermocouple used to monitor temperature is located.

In general, alteration of sample state during preparation, such as by microcracking of the rock during drilling or partial sample dehydration, would lead to measurement of conductivities that were too low. The same is true for any contact resistance that might exist between the heat-probe assembly and the rock. Uncertainties in power output per unit length of heat probe were minimized in these measurements by frequent calibration of the heating probe filament; thermocouple junctions were also frequently checked. Sample inhomogeneities near the central thermocouple are checked for by sawing the sample in half lengthwise after measurement. In one case, sample U12gHEH1B-62 the thermocouple was found to be placed in the center of a porous pumice fragment, making the data collected unusable. It thus appears that possible experimental errors made during measurement

should lead, if anything, to the reporting of conductivities that are too low.

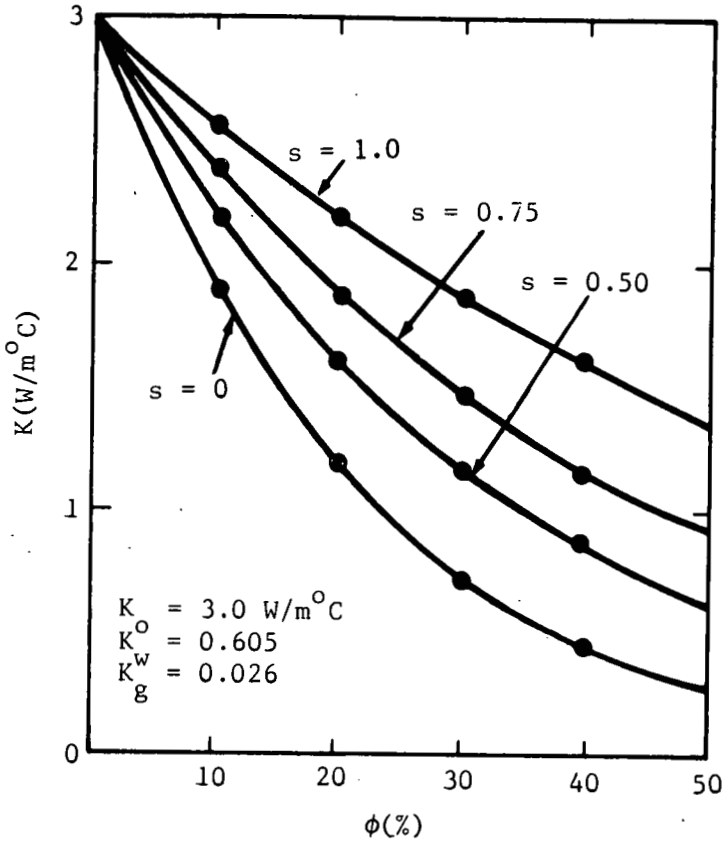

Figure 5. Calculated Rock Conductivity as a Function of Porosity and Saturation When K_o = 3 W/m°C

Results and Comparison of Measured and Calculated Conductivities

During this study, thermal conductivities have been measured on a series of 12 tuffs that were at or near natural-state saturation at the time of measurement. Stratigraphic positions of the samples and both complete and simplified sample identifications are given in Table 2. Simplified identifications are used throughout the rest of the report. Details of the specific measurement conditions and results are given for each test in Tables 3 and 4.

For these 12 tuffs, theoretical matrix conductivity values (K_o) have been calculated according to Equation (3). Results are summarized in Table 5 and shown in Figure 6 as a function of reported grain density.

Sample numbers shown in Figure 6 are keyed to Table 2. Also shown in Figure 6 are some of the theoretical trends of matrix conductivity based on mineralogical considerations alone and taken directly from Figure 4.

Table 2

Stratigraphic Position of Tuffs Studied and Simplified Identifications

Complete Sample ID	Simplified ID	Stratigraphic Position
Ue25A#1-1253	1253	Topopah Springs Member, Paintbrush Tuff
Ue25A#1-1555	1555	Bedded Tuffs of Calico Hills (Local Unit occurring between the Paintbrush and Crater Flat Tuffs)
Ue25A#1-1949	1949	Prow Pass Member, Crater Flat Tuff
Ue25A#1-1966	1966	
Ue25A#1-2341	2341	Bullfrog Member, Crater Flat Tuff
Ue25A#1-2365	2365	
Ue25A#1-2432	2432	
Ue25A#1-2448	2448	
U12g10-HFS30-025.0-25.8	25	Tunnel Bed 4 (Local Unit)
U12g10-INST5#2 21.4-22.0	22	Tunnel Bed 5 (Local Unit)
U12g10-HEH1B-62	62	Grouse Canyon Member, Belted Range Tuff
U12g10-HEH1B-63.4	63	
U12g10-HEH1B-63.8	64	
U12g10-HEH1B-66	66	
U12g10-Ev6#3-81.2-82.3	82	

Table 3

Individual Conductivity Test Results at Ambient Pressure
(Testing Conducted at Holmes and Narver, Inc., Mercury, NV)[23-26]

Sample	Conductivities (W/m°C)			T (°C)		
	25 (NS)*	25 (OD)**	25 (AT)***	110	300	500
1253	2.11	1.86	1.66	1.50	1.39	
	2.07	1.83	1.68	1.43	1.40	
	2.07	1.85	1.68	-	1.41	
1555	1.06	0.81	0.66	0.72	0.68	0.69
	1.10	0.80	0.64	0.71	0.70	0.69
	1.15	0.79	0.64	0.71		0.71
1949	1.74	1.38	1.17	1.36	1.22	
	1.80	1.35	1.14	1.30	1.19	
	1.75	1.36	1.15	1.32	1.20	
1966	1.48	1.19	1.05	1.07	1.05	
	1.47	1.12	1.08	1.08	1.07	
	1.52	1.13	1.08	-	1.07	
2432	2.24	1.48	1.19	1.28	1.31	1.02
	2.18	1.42	1.09	1.28	1.28	1.15
	2.15	1.48	1.12	1.31	-	1.05
25	0.61	-	-	0.43(1)	0.41(2)	0.41(3)
				0.43	0.38	0.41
				0.41	0.38	0.41
				0.43	0.38	
				0.43		
				0.43		
				0.44		
22	0.84	-	-	0.44(1)	0.46(2)	0.46(3)
				0.43	0.49	0.43
				0.42	0.44	0.47
				0.49	0.47	0.41
				0.44		
				0.44		
63	1.45	1.03	0.96	0.99	0.91	-
	1.44	1.04	0.95	0.99	0.91	
	1.46	1.03	0.95	1.00	0.88	
82	1.62	-	-	1.28(1)	1.37(2)	1.21(3)
				1.09	1.23	1.23
				1.10	1.16	1.15
				1.24	1.28	1.21
				1.16		
				1.13		
62	0.99(4)	0.85	0.85	0.87	0.79	-
	1.01	0.89	0.84	0.87	0.81	
	0.99	0.88	0.85	0.86	0.80	

*(NS) = Natural state

**(OD) = Oven-dried, measured before testing at high temperature

***(AT) = Measured after testing at high temperature

(1) Includes measurements made between 105 and 170°C

(2) Includes measurements at both 300 and 350°C

(3) Includes measurements at both 450 and 500°C

(4) ρ_g = 2.62, ϕ = 0.20, S = 0.93. After measurement, central portion of heat probe found to be in center of large, highly porous pumice clot. Data for this sample not included in figures.

Table 4

Individual Conductivity Test Results at Varying Confining Pressures, Pore Pressures, and Temperatures (Testing Conducted at Terra Tek, Inc., Salt Lake City, UT) Reference 27

Conditions			Thermal Conductivity (W/m°C) Sample	
σ_3*(MPa)	p_p**(MPa)	T (°C)	2365	64
0	0	23	2.54	1.48, 1.48
10	9/4***	23	2.26	1.48, 1.51
25	10	23	2.39	1.50, 1.52
50	10	23	2.40	1.42
50	10	150	2.43	
50	10	250	2.16	
50	10	290	2.22, 2.17	
			2448	64
0	0	23	2.67, 2.65	1.55, 1.51
5.5	3.5	23	2.74, 2.77	
10.3	3.5	23	2.61, 2.64	1.50
10.3	3.5	150	2.55, 2.60	1.56, 1.58
10.3	3.5	230		1.64
10.3	3.5	260		1.21, 1.19
10.3	3.5	280	1.67	1.18
			2341	66
0	Dry	23	1.56	0.99
1.5	Dry	275	1.60 (1.98)****	1.15
35	Dry	275	(1.90)	1.24

*σ_3 = Confining pressure

**p_p = Pore pressure

***Two tests, 9 first test, 4 second test.

****Retested after jacket failure.

Table 5

Material Properties and Averaged Conductivity Data for Analyzed Samples (K_{gas} = 0.026 W/m°C)
(Averages Based on Data Given in Tables 3 and 4)

Sample	g/cm ρ_b	g/cm ρ_{db}	g/cm ρ_g	ϕ^*_{calc}	S^{**}_{calc}	W/m°C $K^{natl\ state}_{meas}$	W/m°C K^{calc}_o	W/m°C K^{graph}_o	W/m°C $\Delta_{(calc-graph)}$	Δ/K^{graph}_o	W/m°C K^{deh}_m	W/m°C K^{deh***}_{calc}	W/m°C Δ	Δ/K_{calc}	W/m°C $K^{calc\dagger}_{gas}$
Ue25A#1															
1253	2.39	2.31	2.55	0.09	0.85	2.08††	2.36	2.33	0.03	0.01	1.69	1.57	0.12	0.08	0.06
1555	1.93	1.67	2.46	0.32	0.81	1.10	1.93	1.00	0.93	0.93	0.74	0.49	0.25	0.51	0.10
1949	2.32	2.14	2.63	0.19	0.97	1.76	2.31	2.25	0.06	0.03	1.30	0.98	0.32	0.33	0.11
1966	2.30	2.11	2.62	0.19	0.98	1.49††	1.84	1.85	-0.01	-0.01	1.12	0.82	0.30	0.37	0.13
2341	2.13	1.99	2.70	0.26	0.53	-	-	5.05	-	-	1.74	-	-	-	-
2365	2.21	2.01	2.66	0.24	0.82	2.40††	3.71	3.45	0.26	0.08	-	-	-	-	-
2432	2.33	2.16	2.64	0.18	0.94	2.19	3.03	2.65	0.38	0.14	1.36	1.29	0.07	0.05	0.04
2448	2.21	2.05	2.68	0.24	0.68	2.65††	4.23	4.25	-0.02	-0.01	-	-	-	-	-
G-Tunnel															
25	1.76	1.41	2.44	0.42	0.83	0.61	0.90	1.00	-0.10	-0.10	0.43	0.20	0.23	1.05	0.16
22	1.78	1.32	2.40	0.45	1.00	0.84	1.10	1.00	0.10	0.10	0.44	0.20	0.24	1.20	0.14
63	2.16	1.92	2.62	0.27	0.90	1.45	2.25	1.85	0.40	0.22	0.98	0.67	0.31	0.46	0.10
64	2.04	1.86	2.64	0.30	0.61	1.52††	2.26	2.65	-0.39	-0.15	1.19	0.59	0.60	1.02	0.27
66	2.14	1.97	2.59	0.24	0.71	-	-	2.06	-	-	1.13	-	-	-	-
82	2.30	2.19	2.52	0.13	0.84	1.62	2.03	2.00	0.03	0.02	1.19	1.15	0.04	0.03	0.03

*From $\rho_{db} = \rho_g - \rho_g\phi$

**From $\rho_b = \rho_{db} + S\phi$, substituting for ϕ

††Sample fully resaturated before testing

***Using K_{gas} = 0.026 W/m°C and $K_o = K^{calc}_o$

$$\dagger K^{calc}_{gas} = \left(\frac{K^{deh}_{meas}}{\left(K^{calc}_{o} \right)^{(1-\phi)}} \right)^{1/\phi}$$

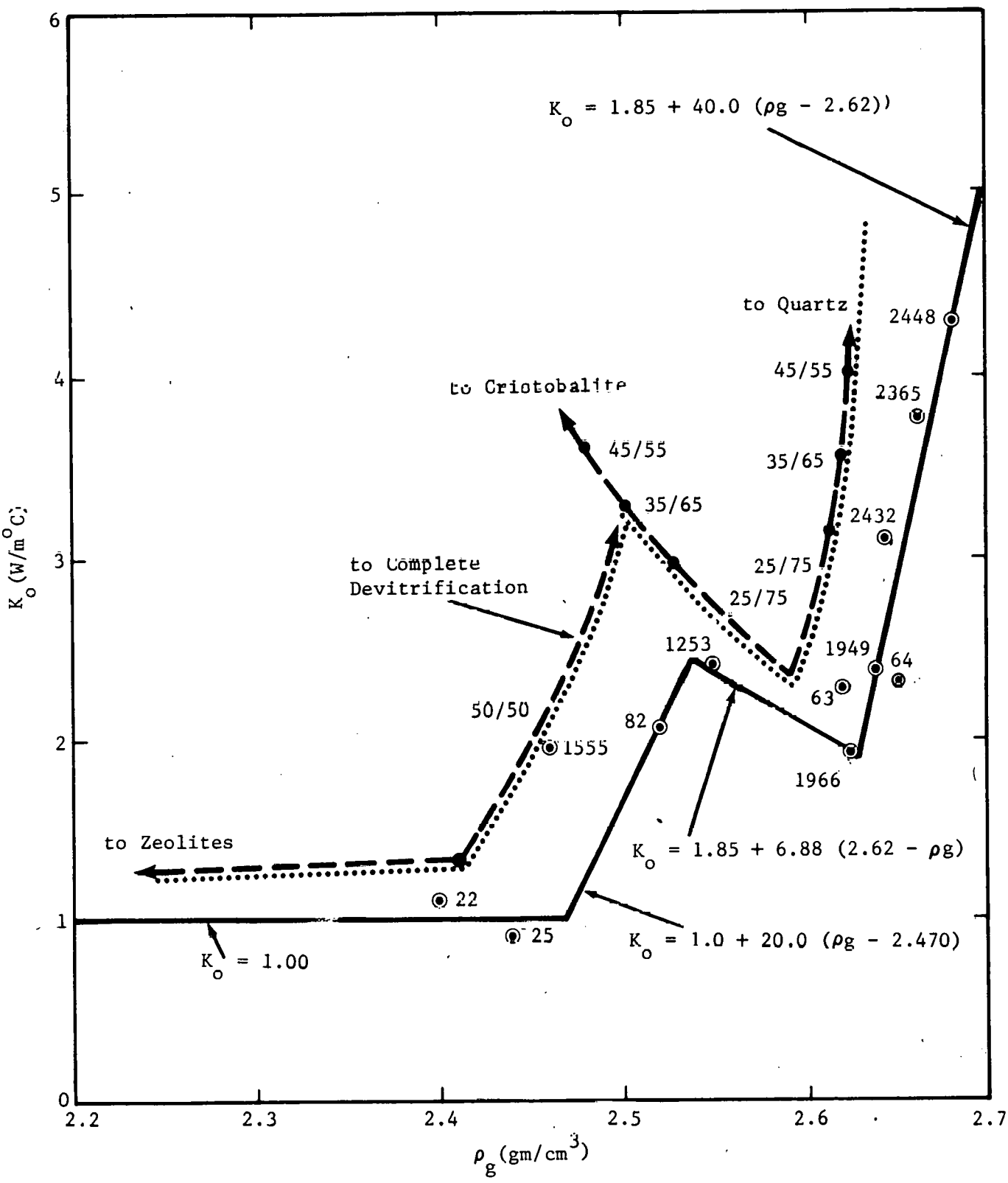

Figure 6. K_o Versus Grain Density for Theoretical Trends and for Experimental Results (Theoretical Curves Taken from Figure 4; see text)

It is immediately apparent that there is qualitative agreement between the theoretical variations in conductivity and limiting boundary curve from Figure 4 and the experimental results, but that at any given grain density calculated K_o values are lower than theoretical values. This is especially true in the case of quartz-bearing samples (grain density greater than 2.60 g/cm^3). In many cases, the difference between theore-tical and extrapolated matrix conductivity for the quartz-rich tuffs is 2 W/m°C or more. Therefore, as in the case of basalts studied by Robertson and Peck,[17] use of the theoretical curves would seriously overestimate tuff conductivity. This is undesirable in waste-management thermal calculations, since it would give results that would not be conservative.

Accordingly, an envelope (indicated by solid lines) has been drawn in Figure 6 that (1) brackets the experimental values of K_o almost entirely on the low side, (2) always lies below the theoretical curve, and (3) is as nearly parallel to it as possible. Use of this envelope to estimate or predict K_o should therefore give conservative results. Specific correlations between ranges of grain density and K_o are indicated for the line segments in Figure 6.

Table 5 indicates that the agreement between the generalized envelope predicting K_o as a function of grain density and the experimental results extrapolated to 0% porosity is within 15% or better, except for two tuffs. In the case of Sample 1555, underestimation of K_o by the bounding curve is due to the fact that the sample, though largely devitrified, is also zeolitized.[11]

Since emplacement of heat-producing wastes in tuff may result in dehydration of the host rock, it is necessary to develop a predictive method for tuff conductivity after dehydration. In theory this should be simple and involve only application of Equation (2) for zero saturation by use of the graphically estimated (extrapolated) values of K_o. Table 5 compares conductivities measured on dehydrated samples with those calculated from Equation (2), by using the experimental K_o values and the literature

gas conductivity value of 0.026 W/m°C.[28] As indicated, use of the textbook value of air conductivity consistently underestimates the dehydrated conductivities with respect to measured values, by an average of 50%.

There are three obvious possible sources of this error:

1. Calculated porosities of most samples may be too high, perhaps as a result of sample preparation procedures
2. The geometric means approach is not valid in tuffs, or
3. The assumption of pure conductive heat transfer across the dehydrated pore spaces is invalid.

One empirical approach to this problem is to use the measured conductivities and saturations to calculate an effective gas conductivity, K_g. Results are shown in Table 5. In the cases of the three samples that were fully saturated before initial conductivity measurement, 1253, 1966 and 64, use of the graphic K_o values and comparison of calculated and measured conductivities of fully dehydrated samples yields calculated gas conductivities of 0.06 (1253), 0.13 (1966) and 0.27 (64) W/m°C. In these cases, no estimation of gas conductivity is required in calculation of K_o. The average gas conductivity calculated for all samples regardless of initial saturation is 0.12 W/m°C. It is therefore assumed that 0.12 W/m°C is a reasonable effective gas conductivity for transfer across the pore spaces in tuffs, and this value is used below.

In order to check the reliability of the estimated K_o values and resultant estimated tuff thermal conductivities, Table 6 compares measured and calculated conductivities of the tuffs studied here. The measured and calculated conductivities of the natural-state and fully saturated samples agree to within an average of 9% ($\pm$11) for all samples, and to within 15% for all samples except 1555. The conductivities of the fully dehydrated samples are predicted within an average of 12% ($\pm$11) for all samples, and to within 14% for all samples other than 1555.

Table 6

Averaged Conductivity Data for Analyzed Samples (K_{gas} = 0.12 W/m°C)

Sample	$K^{natl\ state}_{meas}$ (W/m°C)	$K^{natl\ state*}_{calc}$ (W/m°C)	$\Delta^{(m-c)}$ (W/m°C)	Δ/K_{calc}	K^{deh*}_{meas} (W/m°C)	K^{deh}_{calc} (W/m°C)	$\Delta^{(m-c)}$ (W/m°C)	Δ/K_{calc}
Ue25A#1								
1253	2.08†	2.06†	0.02	0.01	1.69	1.78	-0.09	-0.05
1555	1.10	0.77	0.33	0.43	0.74	0.51	0.23	0.45
1949	1.76	1.74	0.02	0.01	1.30	1.29	0.01	0.01
1966	1.49†	1.50†	-0.01	-0.01	1.12	1.10	0.02	0.02
2341	-	-	-	-	1.74	1.91	-0.17	-0.09
2365	2.40†	2.40†	0.0	0.0	-	-	-	-
2432	2.19	1.99	0.20	0.10	1.36	1.52	-0.16	-0.11
2448	2.65†	2.88†	-0.23	-0.08	-	-	-	-
G-Tunnel								
25	0.61	0.72	-0.11	-0.15	0.43	0.41	0.02	0.05
22	0.84	0.80	0.04	0.05	0.44	0.39	0.05	0.13
63	1.45	1.31	0.14	0.11	0.98	0.88	0.10	0.11
64	1.52†	1.70†	-0.18	-0.11	1.19	1.05	0.14	0.13
66	-	-	-	-	1.13	1.04	0.09	0.09
82	1.62	1.66	-0.04	-0.02	1.19	1.39	-0.20	-0.14

†Measured and calculated at complete saturation

*$K_o = K_o^{graph}$

It remains only to examine the validity of lumping data collected at several pressures and temperatures in calculating K_o values. Figure 7 summarizes dependence of welded-tuff conductivity on effective confining pressure by using data given in Table 3. The results are consistent with the interpretation that the thermal conductivity of either natural-state or fully dehydrated welded tuffs will be insensitive to both confining and fluid pressures to at least 40 MPa, to within the margin of error inherent in the experimental measurements. This conclusion does not consider the elevation of the boiling point of water by increasing confining pressure.

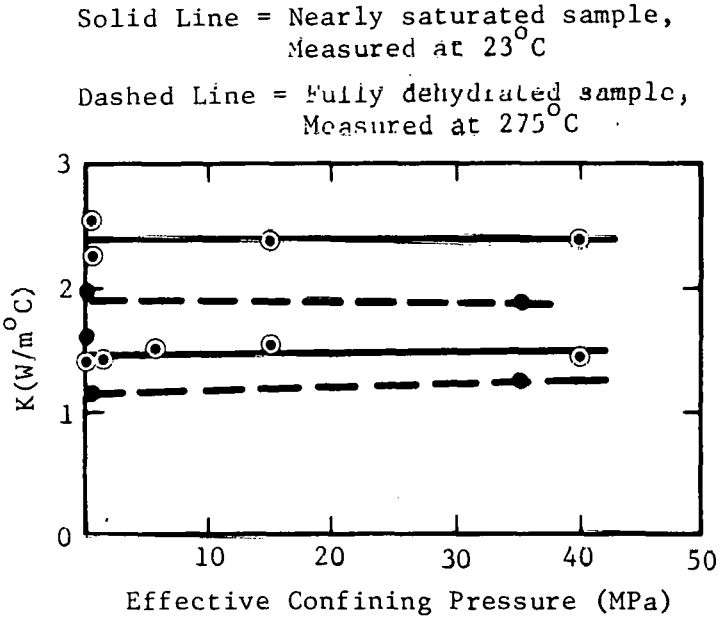

Figure 7. Variations in Tuff Conductivity as a Function of Effective Confining Pressure for Welded Tuffs

Conductivity measurements made as a function of temperature are summarized graphically in Figures 8 and 9. In Figure 8 results are shown for measurements made on natural-state samples under confining pressure at temperatures up to nearly the boiling point of water under the experimental conditions. Results are consistent with the interpretation that the natural-state conductivity of tuffs is effectively insensitive to temperature up to the local boiling point of water.

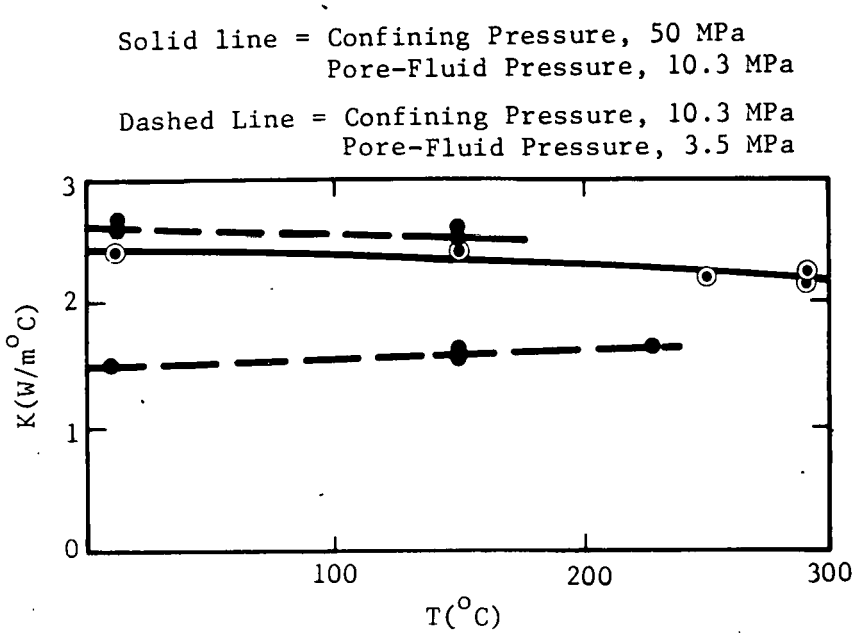

Figure 8. Variations in Conductivity of Welded Tuffs as a Function of Temperature, Below the Boiling Point of Water at Experimental Conditions

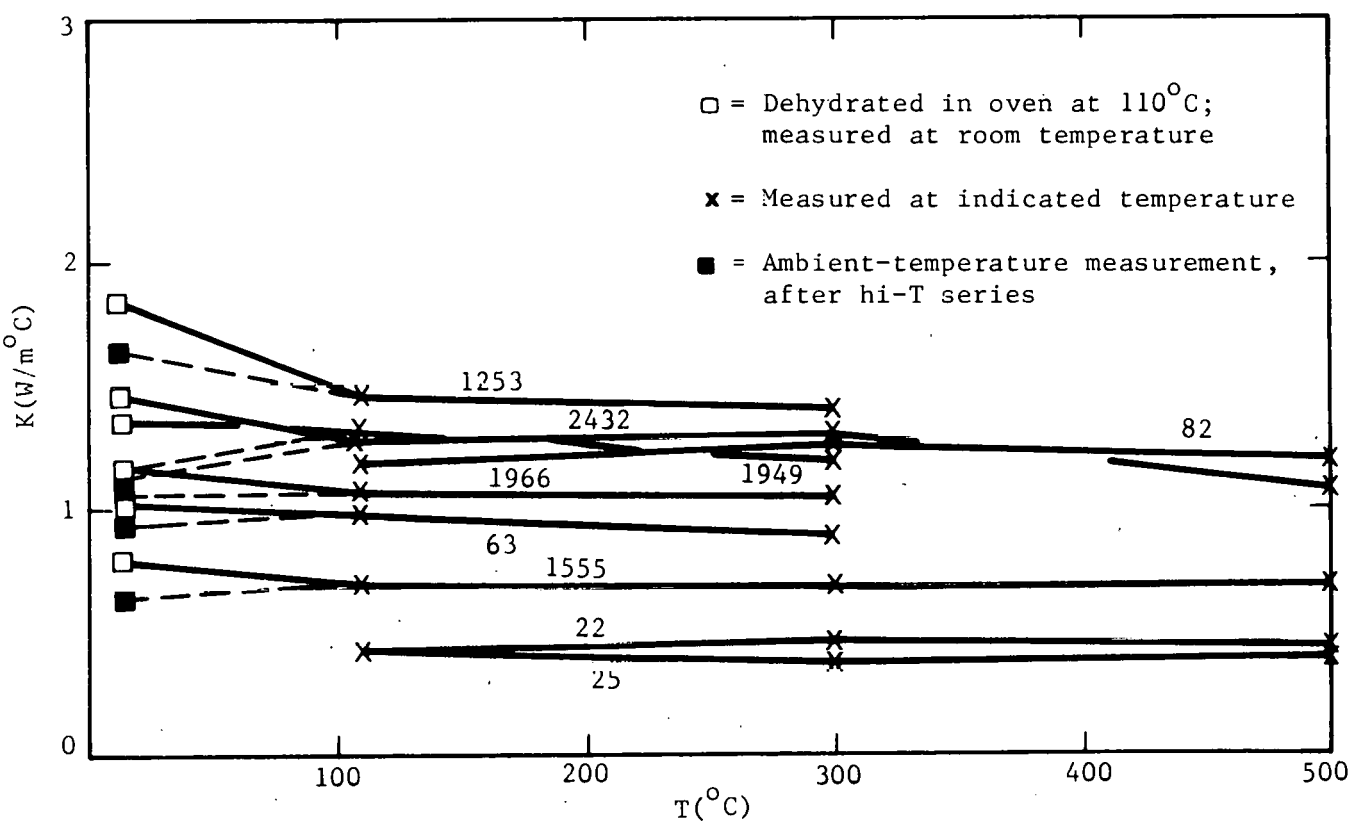

Figure 9. Variations in Thermal Conductivity of Fully Dehydrated Tuffs as a Function of Temperature

Figure 9 summarizes results of ambient-pressure measurements made on fully dehydrated samples as a function of temperature. In general, there is very little sensitivity of conductivity to temperature in the case of the dehydrated rocks. However, in most cases, the ambient-temperature conductivity of oven-dried samples measured before testing at higher temperatures exceeds both the conductivities measured at elevated temperatures and the ambient-temperature conductivity measured after thermal cycling. To estimate K_o values, both the oven-dried and post-testing conductivities have been averaged into the data. The apparent insensitivity of tuff conductivity to temperature for fully dehydrated samples is consistent with the one other study of tuff conductivity at elevated temperatures.[29]

Summary and Conclusions Pertaining to Effort to Develop Tuff Conductivity Formalism

Silicic tuffs are very complex mineralogically and can undergo an almost bewildering array of mineralogical reaction as a result of simple cooling and/or interactions with deuteric water or groundwater. Nonetheless, it is possible to estimate fairly well-defined trends of theoretical matrix conductivity as a function of grain density. Combination of four such trends allows determination of a minimum theoretical matrix conductivity for most tuffs. The four trends are for zeolitization, devitrification, uncertainties in the cristobalite/feldspar ratio of simply devitrified tuffs, and uncertainties in the quartz content of quartz-bearing or microgranitic tuffs. Except for those tuffs that have undergone significant argillic or propylitic alteration, the zero-porosity matrix conductivities of silicic tuffs should lie above this bounding curve. Comparison of measured conductivities with the theoretical results reveals that, while theoretical matrix conductivities extrapolated from laboratory measurements parallel the theoretical curves, they uniformly fall at a lower conductivity at given grain density.

Use of an experimentally determined bounding curve and an effective air conductivity of 0.12 W/m°C allows prediction of both the natural-state and fully dehydrated conductivity of a broad range of tuffs to within 15% or less with a high degree of confidence. This conclusion appears valid to temperatures as high as 300°C and pressures as high as 50 MPa, at least for welded tuffs.

Further comments are in order, however, on the application and possible improvement of the formalism developed here. Accordingly, the different units from which the analyzed tuffs were taken are briefly discussed below as regards their mineralogical variability and its likely consequences on the accuracy of predicted conductivities.

Analyzed samples from the Prow Pass and Bullfrog Members of the Crater Flat Tuff (1949, 1966, 2365, 2432, 2448, see Table 2) have calculated K_o values (see Figure 6) that all fall very near to the bounding curve for quartz-rich tuffs, $K_o = 1.85 + 40.0\ (\rho_g - 2.62)$. This is consistent with the overall mineralogy of samples from this depth range in Hole Ue25A#1.[11] It would thus appear that the predictive curve is reliable for this stratigraphic interval. In Hole J-13, however, the stratigraphically equivalent tuffs are reported to be partially zeolitized.[2] If a tuff had an initial grain density of 2.63 g/cm^3 (equivalent to the density of Sample 1949), 10% zeolitization would decrease the grain density to about 2.59 g/cm^3 and also decrease the expected theoretical matrix conductivity slightly. The graphic K_o value at this lower grain density is only 2.06 W/m°C, however. It thus appears that the predictive curve given should be conservative for partially zeolitized portions of the Bullfrog as well as for those samples analyzed here. The same applies to samples of Bullfrog in which conversion of cristobalite to quartz is reported to be incomplete,[2] since the presence of quartz is totally ignored here for grain densities below 2.62 g/cm^3.

The conductivity of the Bullfrog Member of the Crater Flat tuff appears quite variable. Measured saturated and fully dehydrated conductivities range from 2.19 to 2.65 and 1.36 to 1.74 W/m°C, respectively, but

have all been measured on samples with grain densities of 2.64 g/cm^3 or greater. To date, grain densities and porosities have been measured on 14 samples from the Bullfrog and range from 2.60 to 2.70 g/cm^3; calculated porosities range from 0.18 to 0.26. Based on the predictive curves developed here, predicted conductivities of these tuffs range from 1.41 to 2.91 W/m°C when fully saturated (2.06±0.46 W/m°C) and from 0.96 to 1.91 W/m°C when fully dehydrated (1.44±0.29 W/m°C). These averages are almost certainly low.

Sample 1555 is from the Bedded Tuff of Calico Hills. This local unit of bedded and nonwelded tuffs is some 140 m thick in Hole Ue25A#1, where it occurs both above and below the static water level. The reported petrographic analyses of this interval,[11] and the conductivity results presented here both reflect the complex interaction of devitrification, zeolitization (with slight argillization), and silicification that is possible in nonwelded tuffs (e.g., Reference 14). The resulting rock is not isochemical with the original bulk composition, and its mineralogy may be quite variable over small areas. The bounding curve given in Figure 6 should give minimum conductivities for such rocks (except for significantly argillized samples), but the amount of underestimation may be considerable. In the case of Sample 1555 the natural-state conductivity is underestimated by 43% and the fully dehydrated conductivity by 45%. Improvement of these estimates would appear to require detailed petrography in order to determine the approximate contents of zeolite, glass, devitrification products plus quartz, and clay in samples from this interval. However, as is reflected in the format of the mineralogical work done to date,[11] this is difficult if not impossible in these very fine-grained rocks. More reliable understanding of the thermal conductivity of this interval is important, however, since it could greatly affect the upward release of heat from wastes emplaced at greater depths.

Conductivity of only one sample from within the devitrified Topopah Springs and Tiva Canyon Members of the Paintbrush Tuff has been measured (Sample 1253). The grain density and calculated K_o of this sample are consistent with the theoretical behavior and bounding curve presented here, $K_o = 1.85 + 6.88\ (2.62 - \rho_g)$. More data from devitrified tuffs are

clearly needed. Because the devitrification of welded tuffs is nearly isochemical and thermally activated, there is generally no reason to expect undue difficulty in predicting their conductivity. There are, however, two potential complications. First, devitrification may not be complete in some tuffs, especially at the margins of thick units or in very thin welded units. Secondly, even though such tuffs are commonly situated above the water table, they are not immune to reactions with groundwater since any precipitation must travel through them to reach the static water level.[14] The Topopah Springs in Ue25A#1, though its mineralogy is largely very simple and dominated by complete devitrification, does contain small amounts of zeolite (heulandite) and quartz fracture fillings.[11] This is apparently the result of such groundwater percolation. In addition, some quartz appears to have been formed as a result of slow devitrification.[19] While the presence of quartz would increase matrix conductivity, the presence of zeolite could make the bounding curve in Figure 6 nonconservative in some cases. More information is needed about the distribution of zeolites (and clays) in welded, devitrified tuffs above the water table, though the zeolitization, based on data available to date, appears to be minor.

Samples 22 and 25 are both still quite glassy, containing about 80 and 70% glass, respectively, with 10 to 15% devitrification. Increase in conductivity due to partial devitrification appears to be offset in these samples by hydration of the glass they still contain. In general, however, the results are consistent with the theoretical and bounding curve for very glass-rich rocks.

Thermal conductivity of three samples from the welded Grouse Canyon Member of the Belted Range Tuff in G-tunnel are reported here (63, 64, 82). Sample 82, from the lower margins of the unit, is only partially devitrified. Its measured conductivity and calculated K_o values fall along the suggested bounding curve for partially devitrified samples, $K_o = 1.00 + 20.0\ (\rho_g - 2.470)$. The matrix of Samples 63 and 64 from the upper slightly welded portion of the unit is completely devitrified, though pumice fragments are still partly glassy. The measured grain densities and calculated K_o values suggest that the silica polymorph in

devitrified portions of this unit has inverted to quartz. This would be consistent with the occurrence of perched water tables in the Rainier Mesa area,[14] and is confirmed by X-ray analysis. Based on the limited results to date theoretical matrix conductivity of devitrified portions of the Grouse Canyon Tuff appear comparable to that of the Prow Pass and Bullfrog Members of the Crater Flat Tuff.

References

1. C. S. Ross and R. L. Smith, "Ash-Flow Tuffs: Their Origin, Geologic Relations and Identification," US Geological Society (USGS) Prof. Paper 366 (Washington: Government Printing Office, 1961).

2. G. H. Heiken and M. L. Bevier, Petrology of Tuff Units from the J-13 Drill Site, Jackass Flats, Nevada, LA-7563-MS (Los Alamos: Los Alamos National Scientific Laboratory, 1979).

3. F. M. Byers, Jr., W. J. Carr, D. P. Orkild, W. D. Quinlivan, and K. A. Sargent, "Volcanic Suites and Related Cauldrons of Timber Mountain-Oasis Valley Caldera Complex, Southern Nevada," USGS Prof. Paper 919 (Washington: Government Printing Office, 1976).

4. C. S. Ross and R. L. Smith, "Water and Other Volatiles in Volcanic Glasses," Am Miner 40:1071-1089, 1955.

5. P. W. Lipman, Chemical Comparison of Glassy and Crystalline Volcanic Rocks, USGS Bulletin 1201-D (Washington: Government Printing Office, 1965).

6. D. L. Hoover, "Genesis of Zeolites," pp 275-284 in Nevada Test Site, E. B. Eckel, ed, Geol Soc Am Mem 110, 1968.

7. T. Murase and A. R. McBirney, "Properties of Some Common Igneous Rocks and Their Melts at High Temperatures," GSA Bulletin 84: 3563-3592, 1973.

8. F. Birch and H. Clark, "The Thermal Conductivity of Rocks and Its Dependence Upon Temperature and Composition," Am J Sci, 238: 613-635, 1940.

9. Y. S. Touloukian, R. W. Powell, C. Y. Ho, and P. G. Klemens, "Thermal Conductivity, Nonmetallic Solids," Thermophysical Properties of Matter, (New York: IFI/Plenum, 1970).

10. K. I. Horai, "Thermal Conductivity of Rock-Forming Minerals," J Geoph Res, 76:1278-1308, 1971.

11. M. L. Sykes, G. H. Heiken, and J. R. Smyth, Mineralogy and Petrology of Tuff Units from the UE25A#1 Drill Site, Yucca Mountain, Nevada, LA-8139-MS (Los Alamos: Los Alamos National Scientific Laboratory, 1980).

12. R. L. Smith, "Zones and Zonal Variations in Welded Ash Flows," USGS Prof. Paper 354-F (Washington: Government Printing Office, 1960).

13. M. Kunugi, N. Soga, H. Sawa, and A. Konishi, "Thermal Conductivity of Cristobalite," J Am Cer Soc, 55: 580, 1972.

14. L. V. Benson, "Mass Transport in Vitric Tuffs of Rainier Mesa, Nye County, Nevada," USERDA Paper NVO-1253-10 (Nevada: US Department of Energy, 1976).

15. F. A. Mumpton, ed, "Mineralogy and Geology of Natural Zeolites," Min Soc Am Short Course Notes, v 4 (Washington, DC: Min Soc Am, 1977).

16. R. W. Spengler, D. C. Muller, and R. B. Livermore, Preliminary Report on the Geology and Geophysics of Drill Hole Ue25a-1, Yucca Mountain, Nevada Test Site, USGS Open File Report 79-1244 (Denver, CO: USGS, 1979).

17. E. C. Robertson and D. L. Peck, "Thermal Conductivity of Vesicular Basalt from Hawaii," J Geoph Res, 79: 4875-4888, 1974.

18. W. Woodside and J. H. Messmer, "Thermal Conductivity of Porous Media. II. Consolidated Rocks," Jour. App. Phys., 32:1699-1706, 1961.

19. P. W. Lipman, R. L. Christiansen, and J. T. O'Connor, "A Compositionally Zoned Ash-Flow Sheet in Southern Nevada," USGS Prof. Paper 524-F (Washington: Government Printing Office, 1966).

20. R. L. Hay and R. A. Sheppard, "Zeolites in Open Hydrologic Systems," pp 93-102 in F. A. Mumpton, ed, "Mineralogy and Geology of Natural Zeolites," Min Soc Am Short Course Notes, v 4 (Washington, DC: Min Soc Am, 1977).

21. G. V. Smith, T. S. Pink, J. R. Lawrence, L. A. Woodward, K. Keil, and A. R. Lappin, Preliminary Survey of Tuff Distribution in Esmeralda, Nye, and Lincoln Counties, Nevada, SAND79-1539 (Albuquerque: Sandia National Laboratories, in press).

22. R. L. Maronelli and K. F. Veith, Thermal Conductivity of Rock: Measurement by the Transient Line Source Method, US Bur Mines Rpt Inv. No. 7939 (Washington: Government Printing Office, 1964).

23. Memo from N. B. C. Yelamanchili, Holmes and Narver, Inc., Mercury, NV to A. R. Lappin of Sandia National Laboratories, "Laboratory Report 173: Thermal Conductivity and Physical Properties of Rock Cores from G-Tunnel," July 24, 1978.

24. Memo from N. B. C. Yelamanchili, Holmes and Narver, Inc., Mercury, NV to A. R. Lappin of Sandia National Laboratories, "Laboratory Report 2068: Thermal Conductivity Tests on Tuff Samples from UE25A#1 Drill Hole," July 31, 1979.

25. Memo from N. B. C. Yelamanchili, Holmes and Narver, Inc., Mercury, NV to A. R. Lappin of Sandia National Laboratories, "Thermal Conductivity Tests on Tuff Samples from Drill Hole U12GHH#1," September 14, 1979.

26. Memo from N. B. C. Yelamanchili, Holmes and Narver, Inc., Mercury, NV to A. R. Lappin of Sandia National Laboratories, "Laboratory Report 584: Thermal Conductivity and Physical Properties Test Results on Tuff Specimens from Drill Hole No. UE25A#1," March 12, 1980.

27. R. G. Van Buskirk, D. O. Enniss, and A. H. Jones, Thermal Conductivity and Expansion Properties of NTS Welded Ash-Flow Tuff, TR80-24 (Salt Lake City: Terra Tek, Inc., in preparation).

28. E. R. G. Eckert and R. M. Dicke, Jr., Analysis of Heat and Mass Transfer (New York: McGraw-Hill, 1972).

29. D. R. Stephens, High-Temperature Thermal Conductivity of Six Rocks, UCRL-7605 (Livermore, CA: Ernest Orlando Lawrence Livermore National Laboratory, 1963).

DISTRIBUTION:

US Department of Energy
Asst Secretary
for Defense Programs
Mail Stop SF-066
Washington, DC 20545
Attn: D. C. Sewell (DP-1)

US Department of Energy
Asst Secretary
for Nuclear Energy
Mail Stop 6E-095
Washington, DC 20545
Attn: G. W. Cummingham (NE-1)

US Department of Energy (8)
Office of Nucl Waste Mangement
Mail Stop B-107
Washington, DC 20545
Attn: S Meyers, NE-30
R. G. Romatowski, NE-30
C. A. Heath, NE-30
D. L. Vieth, NE-30
R. Stein, OW, NE-30
C. R. Cooley, NE-30
M. W. Frei, NE-30
G. P. Dix, EV-12, MSE-201

US Department of Energy (2)
Richland Operations Office
PO Box 550
Richland, WA 99352
Attn: F. Standerfer
D. J. Squires

US Department of Energy
Albuquerque Operations Office
PO Box 5400
Albuquerque, NM 87115
Attn: D. T. Schueler, Jr.

US Department of Energy
San Francisco Operations Office
1333 Broadway, Wells Fargo Bldg
Oakland, CA 94612
Attn: L. Lanni

Rockwell International (2)
Atomics International Division
Rockwell Hanford Operations
Richland, WA 99352
Attn: R. Deju
B. Dietz

US Department of Energy (2)
Nevada Operations Office
PO Box 14100
Las Vegas, NV 89114
Attn: M. E. Gates
R. W. Taft
R. W. Newman
J. B. Cotter
M. P. Kunich
H. L. Melancon
A. J. Roberts
R. M. Nelson
D. G. Jackson
P. J. Mudra
R. H. Marks, CP-1
S. R. Elliott
B. W. Church
T. H. Blankenship
R. R. Loux (10)

US Department of Energy (3)
NTS Support Office
PO Box 435
Mercury, NV 89023
Attn: J. H. Dryden
F. Huckabee
L. P. Skousen

DOE Region 9
Director of External Affairs
111 Pine Street, 3rd Floor
San Francisco, CA 94111
Attn: D. J. Cook

US Department of Energy
Columbus Program
Richland Operations Office
505 King Avenue
Columbus, OH 43201
Attn: J. O. Neff

Nuclear Regulatory Commission (2)
Washington DC, 20555
Attn: J. C. Malaro, MS SS674
R. Boyle, MS P-522

Holmes & Narver, Inc.
PO Box 14340
Las Vegas, NV 89114
Attn: A. E. Gurrola

DISTRIBUTION: (CONT)

Lawrence Livermore Laboratory (7)
University of California
PO Box 808
Livermore, CA 94550
Attn: L. D. Ramspott, L-204
A. Holzer, L-209
L. B. Ballou, L-204
J. S. Kahn, L-49
K. Street, L-209
R. C. Carlson, L-204
A. B. Miller, L-204

Los Alamos Scientific Laboratory (6)
PO Box 1663
Los Alamos, NM 87545
Attn: K. Wolfsberg (2)
L. S. Germain, MS 570
L. Lanham, MS 755
J. R. Smyth, MS 978
B. R. Erdal, MS 514

Westinghouse (7)
PO Box 708
Mercury, NV 89023
Attn: D. C. Durrill

Westinghouse - AESD (11)
PO Box 10864
Pittsburg, PA 15236
Attn: J. B. Wright (6)
W. R. Morris
T. E. Cross
R. J. Bahorich
C. R. Bolmgren
W. A. Henninger

University of Arizona
Nuclear Fuel Cycle Research
Tucson, AZ 85721
Attn: J. G. McCray

US Geologic Survey (3)
National Center
Reston, VA 22092
Attn: G. D. Debuchananne, MS 410
P. R. Stevens, MS 410
D. B. Stewart, MS 959

US Geologic Survey (2)
PO Box 25046
Federal Center
Denver, CO 80225
Attn: G. L. Dixon, MS 954
W. S. Twenhofel, MS 954

Geologic Society of America
3300 Penrose Place
Boulder, CO 80302
Attn: J. C. Frye

University of Kansas
Kansas Geological Survey
Lawrence, KS 66044
Attn: W. W. Hambleton

Battelle (10)
Office of Nucl Waste Isolation
505 King Avenue
Columbus, OH 43201
Attn: N. E. Carter
S. Basham
J. Carr
ONWI Library (5)
R. A. Robinson
W. Carbiener

State of Nevada
Governor's Office of Planning
Coordination
Capitol Complex
Carson City, NV 89710
Attn: R. Hill, State
Planning Coordinator

Fenix & Scisson, Inc.
PO Box 498
Mercury, NV 89203
Attn: F. D. Waltman

State of Nevada
Capitol Complex
Caron City, NV 89710
Attn: N. Clark,
Dept of Energy

Woodward-Clyde Consultants
Western Region Library
No. 3 Embarcardero Center
San Francisco, CA 94111

DISTRIBUTION: (CONT)

John A. Blume Engineers
Sheraton Palace Hotel
130 Jessie Street
San Francisco, CA 94105
Attn: P. Yanev

Harvard University (2)
Dept of Earth Sciences
Cambridge, MA 02138
Attn: R. Siever

Dartmouth College
Dept of Earth Sciences
Hanover, NH 03755
Attn: J. Lyons

Internatl Atomic Energy Agency
Div of Nucl Power & Reactors
Karntner Ring 11
PO Box 590, A-1011
Vienna, Austria
Attn: J. P. Colton

Fenix & Scisson, Inc.
PO Box 15408
Las Vegas, NV 89114
Attn: J. A. Cross

California Energy Resources
Conservation & Devel Com
1111 Howe Avenue
Sacramento, CA 95825
Attn: A. Soinski

University of California
Lawrence Berkeley Laboratory
Energy & Environment Division
Berkeley, CA 94270
Attn: P. Witherspoon

Hanford Eng Development Lab
PO Box 1970
Richland, WA 99352
Attn: D. Cantley

Princeton University
Dept of Civil Engineering
Princeton, NJ 08540
Attn: G. Pinder

Arthur D. Little, Inc.
Acorn Park
Cambridge, MA 02140
Attn: C. R. Hadlock

Brown University
Dept of Geological Sciences
Providence, RI 02912
Attn: B. Giletti

Texas A&M University
Center for Tectonophysics
College Station, TX 77840
Attn: J. Handin

Law Engineering Testing Co.
2749 Delk Road, SE
Marietta, GA 30067
Attn: B. Woodward

Holmes & Narver, Inc.
PO Box 1
Mercury, NV 89023
Attn: G. E. Christensen

Subcommittee on Energy
Research & Production
Room B-374
Rayburn House Office Bldg
Washington, DC 20575
Attn: S. Lanes, Staff Dir.

Dept of Health and Environment
Bureau of Radiation Control
Forbes Field
Topeka, KS 66620
Attn: G. W. Allen, Director

State of Connecticut
Energy Research and Policy
80 Washington Street
Hartford, CT 06115
Attn: F. N. Brenneman

State of Michigan
Office of the Governor
Executive Office
Lansing, MI 48909
Attn: W. C. Taylor
Science Advisor

DISTRIBUTION: (CONT)

Dir for Policy and Planning
325 West Adams St - Room 300
Springfield, IL 62706
Attn: A. Liberatore

Nuclear Energy Division
Nucl Projects Coordinator
PO Box 14690
Baton Rouge, LA 70808
Attn: L. H. Bohlinger

Oregon Dept of Energy
Labor & Industries Bldg
Room 111
Salem, OR 97310
Attn: D. W. Godard

Radiation Protection Div
1000 Northeast 10th Street
PO Box 53551
Oklahoma City, OK 73152
Attn: R. L. Craig, Dir

Reynolds Elect & Eng Co., Inc. (7)
PO Box 14400
Las Vegas, NV 89114
Attn: H. D. Cunningham, MS 555
W. G. Flangas, MS 615
G. W. Adair, MS 154
V. M. Milligan, MS 765
C. W. Dunnam, MS 745
R. L. Powell, MS 634
R. B. Land, MS 585

Radiation Health Info Project
Environmental Policy Inst
317 Pennsylvania Ave, SE
Washington, DC 20003
Attn: E. Walters

State of South Carolina
Div of Energy Resources
Edgar A. Brown Bldg
1205 Pendleton Street
Columbia, SC 29201
Attn: L. E. Priester, Jr.

Federal Agency Relations
1050 17th St, NW
Washington, DC 20036
Attn: O. H. Davis, Dir

Environmental Program Supvr
903 Ninth Street Office Bldg
Richmond, VA 23219
Attn: K. J. Buttleman

Energy Administration
Dept of Natural Resources
Tawes State Office Bldg
Annapolis, MD 21401
Attn: P. Massicot, Actg Dir

State of Ohio Environmental
Protection Agency
361 E. Broad St - Box 1049
Columbus, OH 43216
Attn: J. F. McAvoy, Dir

State of Connecticut
House of Representatives
One Hundred and Sixth District
24 Rock Ridge Road
Newtown, CT 06470
Attn: J. W. Anderson

MO Dept of Natural Resources
PO Box 176
Jefferson City, MO 65102
Attn: T. D. Davis

MS Dept of Natural Resources
Suite 228, Barefield Complex
455 North Lamar Street
Jackson, MS 39201
Attn: P. T. Rankston

Tennessee Energy Authority
Suite 708 Capitol Blvd Bldg
Nashville, TN 37219
Attn: J. A. Thomas, Assoc Dir

Council Member
374 South Rock River Drive
Berea, OH 44017
Attn: G. A. Brown

Public Law Utilities Group
One American Pl, Suite 1601
Baton Rouge, LA 70825
Attn: D. Falkenheier, Asst Dir

Energy Facility Site Eval Council
820 East Fifth Ave
Olympia, WA 98504
Attn: N. D. Lewis

DISTRIBUTION: (CONT)

Georgia Institute of Technology
Associate Dean for Research
Atlanta, GA 30332
Attn: R. Williams

University of Texas at Austin
University Station, Box X
Austin, TX 78712
Attn: E. G. Wermund

Dept for Human Resources
Commonwealth of Kentucky
Frankfort, KY 40601
Attn: R. M. Fry

Office of Energy Resources
73 Tremont Street
Boston, MA 02108
Attn: L. Morgenstern

Dept of Environmental
Regulation
Twin Towers Office Bldg
2600 Blair Stone Road
Tallahassee, FL 32301
Attn: D. S. Kell

1112 C. R. Mehl
Attn: C. W. Smith
1417 F. W. Muller
1417 G. F. Rudolfo
1762 M. R. Zimmerman
4413 N. R. Ortiz
Attn: F. Donath
4500 E. H. Beckner
4510 W. O. Weart
4530 R. W. Lynch
4537 L. D. Tyler
4537 J. K. Johnstone
4537 B. S. Langkopf
4537 A. R. L. Lappin (35)
4538 R. C. Lincoln
4538 S. Sinnock
4540 M. L. Kramm
4550 R. M. Jefferson
5510 D. B. Hayes
5511 J. W. Nunziato
5521 L. W. Davison
5521 R. K. Thomas
5532 B. M. Butcher
5532 W. A. Olsson
5541 W. C. Luth
5541 J. C. Eichelberger
5824 J. N. Sweet
5824 M. Moss
8266 E. A. Aas
3141 T. L. Werner (5)
3151 W. L. Garner (3)
For DOE/TIC (Unlimited Release)
DOE/TIC (25)
(R. P. Campbell, 3154-3)

Org.	Bldg.	Name	Rec'd by *	Org.	Bldg.	Name	Rec'd by *

* Recipient must initial on classified documents.